Development of a High Performance Natural Gas Engine with Direct Gas Injection and Variable Valve Actuation

2017-24-0152

Development of a High Performance Natural Gas Engine with Direct Gas Injection and Variable Valve Actuation

Author, co-author (Do NOT enter this information. It will be pulled from participant tab in MyTechZone)

Affiliation (Do NOT enter this information. It will be pulled from participant tab in MyTechZone)

Abstract

Natural gas is a promising alternative fuel for internal combustion engine application due to its low carbon content and high knock resistance. Performance of natural gas engines is further improved if direct injection, high turbocharger boost level, and variable valve actuation (VVA) are adopted. Also, relevant efficiency benefits can be obtained through downsizing. However, mixture quality resulting from direct gas injection has proven to be problematic. This work aims at developing a mono-fuel small-displacement turbocharged compressed natural gas engine with side-mounted direct injector and advanced VVA system. An injector configuration was designed in order to enhance the overall engine tumble and thus overcome low penetration. Gas injection, interaction thereof with charge motion and geometrical bounding walls, and the resultant mixture formation process was investigated in detail by the combination of planar laser-induced fluorescence (LIF) in an optical engine and computational fluid dynamics (CFD) analysis with moving injector model to verify the design of the injector and combustion chamber. Then a prototype engine was tested to compare the rated torque against target performance. The planar LIF investigation underlined the influence of the Coandă effect whereby the gas jet was deflected to the adjacent injector niche and then to the combustion chamber roof. Such effect was inhibited at early injection timings due to strong intake air flow. CFD analysis confirmed this behavior and pointed out that the mixing process is dominated by the gas jet during injection and flow patterns promoted by it. It was concluded that the principal mixing mechanism is the jet-promoted tumble and elliptical swirl motion, and the mixing rate is thereby scaled with absolute time, rather than crank angle degree, and mainly determined by the strength of these two motion patterns. It was in addition found that the injection contributes to combustion-relevant turbulence mainly by intensifying the large-scale charge motion. Overall high mixing capacity was observed, and the injector and combustion chamber design deemed efficacious. The engine design has been successfully accomplished and the prototype multi-cylinder engine (MCE) is ready for extensive performance and emission analysis on the test rig.

Introduction

As internal combustion (IC) engines are still considered as the major technical solution to the sustenance of the rising demand for contemporary human mobility, while extensive adoption and growing performance request of IC engines are observed, the accompanying drawbacks, especially those detrimental to natural resources and environment, have to be appropriately addressed. In this regard, increasingly stringent regulations on pollutant and CO_2 emissions have been imposed on IC engines, which have encouraged the energy and transportation industries to seek new technologies applicable to the conventional engine concepts or to resort to alternative combustion systems. Such a trend is expected to continue in the future.

Natural gas (NG) is deemed one of the most promising alternative fuels, which, in conjunction with suitable engine optimization, can effectively cope with the concerns pertaining to conventional IC engines by reducing pollutant emissions as well as the crude-oil dependence on a significant scale [1,2]. NG is in nature a gaseous fossil fuel and consists of various gas species. The availability of NG is warranted by many discovered yet unexploited gas reservoirs, sustainable fuel synthesis methods under constant development, the production of bio-methane from biomass gasification, and the exploitation of shale gas [3,4,5]. The prominence of NG as an alternative fuel to gasoline for spark-ignition (SI) engine application is attributable to its peculiar properties that are very similar to methane, the primary and determinative constituent of NG. Methane has the highest molecular hydrogen-to-carbon ratio of all hydrocarbons, which lowers its CO_2 footprint as compared to the long-chained molecules found in conventional fuels. Another attractive chemical property of methane is its research octane number of 130 which is considerably higher than that of gasoline. This indicates high knock resistance as a critical enabling factor, generally eluding gasoline due to the adverse effect of knocking, for extracting more power from a given engine displacement and therefore increasing engine specific power. In particular, NG engines operating with high compression ratio and boost pressure level as well as lean-burn approach or heavy exhaust gas recirculation could be equivalent to, or even outperform, their gasoline counterparts in terms of torque and power while allowing of a substantial reduction in pollutant emissions and improvement in engine thermal efficiency [1,6,7]. Furthermore, the physical property of NG, being in gaseous state in engine operating conditions, gives rise to better combustion completeness and intrinsically avoids the risk of wall wetting.

On the basis of the characteristics of NG as an alternative fuel, NG engine performance can be further improved by utilizing direct injection (DI) as the fueling method. Port fuel injection (PFI) is currently the dominant fuel supply method for NG engines wherein the injected gaseous fuel inside the intake ports displaces a perceivable portion of fresh air volume before entering the combustion chamber. Therefore the adoption of DI can bring forth

the benefits of increase in volumetric efficiency and hence in engine torque [2,8]. Moreover, without the premixed intake charge, engines working with DI have the flexibility of postponing the injection event and thus can take advantage of clearance-volume scavenging. This is effective in ameliorating volumetric efficiency and compressor operating conditions at low engine speeds. NG engines with DI, in addition, have shown potential for enhancing combustion characteristics and extending the lean-burn operating limit in comparison with PFI engines [1,9]. Direct gas injection, despite the apparent advantages, poses critical challenges in obtaining adequate control of air-fuel mixture quality when a NG DI combustion system is to be designed, mainly as a result of the fuel being constantly in gaseous state with low mass density [10,11,12]. Mixture quality, however, has well-known crucial influence on the combustion efficiency and emissions, especially that of total HC for SI engines.

In pursuit of establishing guidelines pertaining to the challenging direct NG injection in IC engine applications, many researches, both experimental and numerical, have been carried out with respect to NG DI engine. Douailler et al. [12] highlighted the impact of gaseous fuel injection on the volumetric efficiency through experiments on a single-cylinder NG SI engine. Zeng et al. [9] conducted an experimental study on the influence of different injection timings on combustion characteristics and engine performance at a given engine speed with fixed injected fuel quantity and spark timing, whereby drawbacks of over-late injection due to insufficient mixing time were pointed out and the existence of an optimum injection timing at that specific engine speed was identified judging by combustion speed and emissions of HC and CO. Mohammed et al. [13] experimentally investigated the effect of injection timing on engine characteristics and emissions of a stoichiometric single-cylinder NG engine at different engine speeds, and concluded that the optimum injection timing for engine performance ought to be advanced as engine speed increased. Aziz and Firmansyah [14] studied the effect of rail pressure, in the medium range for NG DI application, on engine performance. It was discussed that higher rail pressure led to better engine performance at lower engine speed due to the predominant influence of volumetric efficiency on combustion, whereas lower rail pressure was preferable at higher engine speed because air-fuel mixing rate was the limiting factor. The experimental study carried out by Chiodi et al. [11] demonstrated the possibility of supporting combustion process with late gas injection of which the kinetic energy induced additional turbulence to accelerate the flame propagation, and found moreover that such mechanism was affected by the valve shape, location and orientation in the case of a side-mounted injector. A numerical study on the mixture preparation in a NG engine with different combustion chamber shapes and centrally mounted injector types was performed by Yadollahi and Boroomand [15], which emphasized the necessity of matching combustion chamber geometry, injection timing, injector type and location for optimum combustion. Keskinen et al. [16] utilized numerical models of sector mesh to study injection-related variables, such as injector nozzle type, injection timing and pressure, and the effects of them on mixture formation at one part-load operating point. The results suggested that injection timing had considerable influence on mixing rate and the mixing mechanism dependent on the nozzle type.

Despite those researches, relevant data on the direct gas injection and subsequent mixture formation for NG engine application remain scarce. The present study, therefore, seeks to provide a detailed fluid-dynamic characterization from the perspective of air-fuel mixing process of a turbocharged CNG SI engine by means of conjoint experimental and numerical investigations. Furthermore, as optimum combustion process results from the combinative effect of various design parameters, this work also aims to give information on the combustion system development as a whole by thoroughly examining the interaction among gas injection, charge motion, and combustion chamber shape at different engine speeds and loads.

Currently the vast majority of compressed NG (CNG) vehicles use bi-fuel engines originally designed to operate with gasoline, wherein the CNG mode consists in the inclusion of a NG PFI system. While the usual choice of remaining gasoline-compliant is ascribable to the lack of CNG-related infrastructure, the bi-fuel NG operation suffers from perceivable performance compromise in comparison with CNG-optimized counterpart [8]. To overcome such situation, the European Commission has promoted a number of research projects in the fields of gas storage, gas feeding, and after-treatment systems. The present study context is the outcome of joint research activities carried out by Politecnico di Torino, Centro Ricerche Fiat, AVL, and Delphi within the GasOn project of the European Commission H2020 program. The overall objective is to develop a mono-fuel small-displacement turbocharged CNG engine, equipped with advanced variable valve actuation (VVA) MultiAir system and direct gas injector, which is able to comply with post-Euro VI emission regulations and post-2020 CO_2 emission targets taking into account the new homologation cycle and real driving conditions.

The current paper is organized in such a way that, firstly, an overview of the main characteristics introduced to the specific CNG DI engine in question is provided, and then the methodology of experimental and numerical investigation to analyze the combustion chamber design are described. Specifically, the mixture formation process was experimentally inspected in an optical engine through planar laser-induced fluorescence (LIF) and the corresponding combustion data were measured, whereas the mixing rate, mixture homogeneity as well as jet-induced turbulence and interaction thereof with charge tumble motion was investigated by numerical simulations. The subsequent section is dedicated to the results and discussion about the engine development concerning the gas injector implementation, the characterization of the air-fuel mixing process and interaction of gas injection with engine flow, and engine performance optimization by bench-testing a multi-cylinder prototype engine. Finally, conclusions on the analysis and achievement of engine development are drawn.

Engine Overview

The CNG engine under question is derived from a 1.4-litre four-cylinder gasoline DI (GDI) engine core and dedicated to NG combustion system optimization, with the strategy of homogeneous stoichiometric charge SI combustion that permits the use of conventional three-way catalytic converter to meet the Euro VI emissions regulations. The small displaced volume, together with a turbocharger, allows considerable downsizing for increase in engine efficiency. The VVA Multiair system is introduced not only to de-throttle the engine, but to be optimized in conjunction with the turbocharger so that the engine flow supports the latter to deliver requested boost while improving the compressor operating point and hence efficiency.

Another important characteristic is the engine architecture of high structural strength able to sustain very high combustion peak pressures (up to 150 bar for a limited period), in order to fully exploit the high knock resistance of NG. Being considerably less prone to knocking, NG engines can eliminate the constraint, i.e. delaying the spark advance from the maximum torque/efficiency timing in gasoline operation mode, and in general adopt more advanced SA that results in a decrease in specific fuel consumption. Apart from the

SA optimization, the robust engine structure also accommodates margin for higher CR, thereby further increasing the efficiency and enhancing performance by favoring peak pressure at rated torque. Accordingly, the combustion chamber is redesigned to raise the CR up to 13.

With respect to the DI, a side-mounted gas injector, with an outward-opening poppet valve, is preferred to a centrally mounted one. From the viewpoint of cylinder head design, placing the injector on the side avoids the interference of the injector housing with valves and the spark plug, therefore simplifying the position arrangement and, more importantly, improving the mechanical strength of the cylinder head. Furthermore, without severe impact on the structural integrity, a larger injector tip is allowed in the side position so as to, given the same injection pressure, deliver a higher mass flow rate as generally required by gaseous fuel applications.

The pent-roof shaped cylinder head, including the side-mounted injector niche between the intake valves, and the piston featuring a shallow bowl are schematically shown in Figure 1. The objective is to achieve the performance equivalent to the boosted GDI version with the same displaced volume. Furthermore, a 20% improvement in fuel economy is expected in comparison with the Fiat in-production CNG PFI engine that has been installed on the B-segment CNG vehicles since 2014. Upon the completion of calibration activities of the prototype engine, demo vehicles will be available for full assessment.

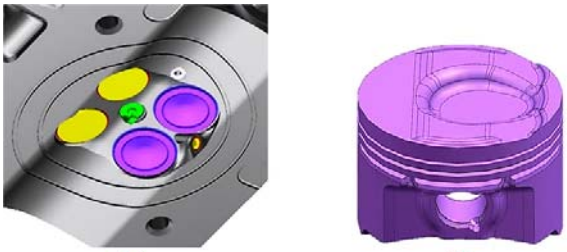

(a) (b)

Figure 1. Combustion chamber of the developed NG engine: (a) cylinder head; (b) piston

Methodology

Experimental Setup

The jet evolution and mixture formation process was experimentally investigated in an optically accessible engine with the planar LIF technique [17]. LIF is a spectroscopic method based on the excitation of molecules of a predetermined species, called tracer, to a higher energy state through selective absorption of photon (the laser pulse) followed, in a few nanoseconds or microseconds, by the spontaneous de-excitation through the emission of another photon at a longer wavelength, i.e. the fluorescence. Typically, excimer lasers, pulsed lasers in the ultraviolet (UV) region of the spectrum with relatively low energy but high pulse repetition, are adopted for LIF experiments owing to their well-defined wavelengths.

With reference to the full engine under consideration, an optical single-cylinder version was built according to the same combustion chamber and ports design, except for the major modification to the metallic liner that was replaced by a transparent one made of glass for lateral optical accessibility. Therefore, the cylindrical glass liner was constantly exposed to the environment and no cooling was supplied. It is worth being underlined that the glass liner imposed some constraints to the experimental procedures. Specifically, the engine could be operated only for a limited number of cycles, especially at high load. For this reason, the engine was firstly motored, and, when all the relevant parameters were set, combustion was enabled for about 200 cycles of which only the latest 50 were measured, so as to ensure that the actually measured cycles correspond to steady state conditions to the greatest possible extent. It is inevitable that the liner temperature was on one hand different from that in the full engine, and on the other hand more dependent on the investigated operating points. Although the combustion behavior was not fully comparable to that in the full engine, the effect of injection timing at given speed and load was still meaningful.

The double-sided planar LIF was implemented in the investigation, wherein via a system of lenses and mirrors a krypton fluoride (KrF) excimer laser beam (wavelength 248 nm) was reshaped and evenly split into two planar light sheets that were then coupled into the same symmetry plane of the combustion chamber from two opposite sides through the glass liner. Such arrangement guaranteed symmetrical illumination of the target symmetry plane which is the vertical plane passing through the cylinder central axis and leaving one intake valve and one exhaust valve on each side. Figure 2 shows the optical engine configuration including the glass liner and one of the two final lenses of the laser path used to illuminate the target plane.

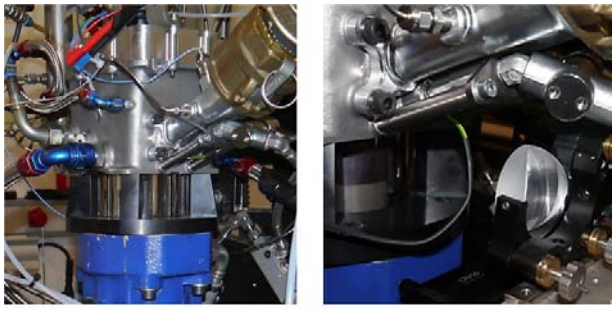

(a) (b)

Figure 2. Planar LIF experimental setup: (a) optical single-cylinder engine; (b) last lens used to couple the light sheet from the intake side

The optical engine was fueled by methane uniformly premixed with 4000 ppm of trimethylamine, $N(CH_3)_3$ or TMA, as the tracer for LIF visualization. TMA was considered to be a suitable tracer in this application thanks to its branched molecular structure giving rise to a large number of excitable energy states for a broadband excitation by the KrF excimer laser at the wavelength of 248 nm, the wavelength at which methane and nitrogen do not absorb light. The subsequent emission fluorescence at the wavelength of about 300 nm was imaged by an intensified charge-coupled device (ICCD) camera with an image-intensifier quantum efficiency of around 20% at 300 nm and an UV-compatible Micro Nikkor lens.

The tracer molecules residing in the laser-illuminated plane during laser pulse would emit fluorescence and be detected by the camera that was placed perpendicular to that plane. The intensity scale of the detected fluorescence emission correlates with the local tracer concentration and, having uniformly mixed together, with the gaseous fuel concentration in the laser-illuminated plane [18]. The acquired LIF images are in grayscale representing the fluorescence intensity detected by the camera. The grayscale is hence qualitatively related to the mixture equivalence ratio, with the brighter being rich and the darker lean. An accurate quantitative interpretation of the correlation between detected luminosity and equivalence ratio requires dedicated multiple LIF measurement and calibration

procedures. That is outside the scope of the present work and will be the subject of a companion paper. LIF images thus acquired, however, were in fact the superimposition of the fuel LIF response and the background signal, both of which, in addition, were affected by the local gain variation. Therefore, additional procedures were necessary to correct the acquired images. Specifically, at each crank angle where the LIF image, named raw LIF image hereafter, was acquired, an image with no tracer in the fuel under otherwise the same conditions, named dark measurement, was also acquired in order to remove the background offset. To compensate the local gain, a LIF image of a homogeneous air-fuel mixture, called reference measurement, and another LIF image of the same mixture but without the tracer, called dark reference measurement, were acquired at all crank angles of interest. The latter dark reference image was actually needed to remove the background offset of the former reference image. Finally the raw LIF images were corrected according to the following expression that isolates the pure fuel LIF response:

$$LIF = \frac{raw\,LIF - dark}{reference - dark\,reference} \quad (1)$$

Furthermore, in the present engine application, the gas jet was subject to intrinsic cycle-to-cycle variation (CCV) since the jet itself was in general highly turbulent. Moreover, compressibility effect of the high-velocity gas flow led to high sensitivity of the jet evolution to CCV of the back pressure in the combustion chamber. Consequently, 35 single LIF images were acquired for each predetermined crank angle and the average image was derived in order to represent the situation with respect to the "ensemble-averaged" engine cycle. With reference to equation 1, the 35 repetitions were done for all the four types of LIF images, and the average images of each type were derived separately prior to the final raw image correction.

Numerical Model

A supplementary three-dimensional computational fluid dynamics (CFD) analysis was undertaken in order to reveal further details about the gas jet and air-fuel mixing characteristics that were otherwise scarcely accessible to experimental investigations.

For the purpose of investigating the gas injection and subsequent air-fuel mixing process in conjunction with the planar LIF visualization, the computational domain encompassed the same engine geometry as that in the LIF experimental setup. Given the geometric symmetry of the combustion chamber and ports about the laser-illuminated plane, only half of the engine volume was considered. The finite-volume numerical model of the engine was developed within the AVL FIRE environment and, with the moving grid, faithfully reproduced the combustion chamber geometry as well as the movement of the piston and valves so as to enable the simulation of real engine cycle.

A particular challenge of the numerical modeling consisted in the simulation of direct gas injection, as a result of the high nozzle pressure ratio (NPR) and substantial geometric scale separation between the injector nozzle and the combustion chamber normally of two orders of magnitude, which essentially involved the widely studied case of high-velocity underexpanded jet [19,20]. Specifically, the supersonic flow region and the formation of shock structures typically occurring with the underexpanded jet emanating from a choked nozzle are acknowledged to be computationally problematic. The situation becomes more critical when the underexpanded jet issues from a gas injector featuring outward-opening poppet valve rather than an axisymmetric orifice. In fact, the latter generates a circular gas jet and the former a hollow cone jet that, depending on the injector geometry and NPR, may shortly collapse to the nozzle axis, maintain the conical shape onwards, or attach to adjacent walls [21,22]. Moreover, the cross section of the injector nozzle in reality varies with time during transient phases as the needle valve opens or closes. Such variation is often complex since, along with the needle valve movement, not only the cross sectional area of the nozzle but also the absolute location of the nozzle throat changes. Many studies have investigated the hollow cone jets ejected from poppet-valve type injectors by means of fixed injector needle lift [12,15,16,22]. It was found, in consequence, that the injector flow initialization through gradual increase in inlet boundary pressure and the location of the boundary are crucial to the numerical model predictability [21]. In addition, during the transient phases the absence of needle valve movement results in lower jet velocity at the nozzle exit and lower jet penetration as a result [12,21].

To improve the fidelity of the numerical model, the time-dependent variation of the injector nozzle was retained in the present study by a dedicated injector model that was manually built as an axisymmetric structure consisting of hexahedral cells. The needle valve in the injector model, imposed as the inner wall boundary of the nozzle, can move according to any given needle lift curve and thus adapts the mesh to the real nozzle geometry at every time instant during the transient phases. Therefore no artificial treatment in the inlet pressure boundary was required to take into account the build-up phase during needle valve opening. The injector model includes the nozzle, a portion of the injector internal path upstream leading to the inlet pressure boundary, and a volume of the combustion chamber immediately downstream in which high grid density is dictated by the supersonic underexpanded jet to resolve with adequate accuracy the large gradient of fluid variables along the flow direction and the expansion fan perpendicular to the flow direction departing from the nozzle exit [23,24]. The inlet pressure in this injector model was obtained by an experimentally calibrated one-dimensional CFD model that monitored the fluid pressure at the same inlet boundary position as a function of the needle lift.

The injector model was embedded in the abovementioned engine moving grid through an arbitrary boundary, a mathematical treatment on the interface between two separate domains across which the values of cell face fluxes are calculated by area-weighted averaging thus mathematically connecting the two domains. It should be noted that the grid embedding was implemented only during the injection event and a short period afterwards, whereas the engine grid encompassing the whole geometric volume, including that reserved for the injector grid, was used otherwise. This strategy ensured the fulfilment of the grid resolution requirement for the gas injection while optimizing the overall computational costs. Given the fact that the cells in the injector grid were much smaller than those in the engine grid, a gradual transition of cell size surrounding the arbitrary boundary interface on the engine side was built. Figure 3 shows the injector grid and three examples of the final computational grid used for the engine simulations in this work, in which the absence and presence of the embedded injector grid, depending on the specific injection timing under investigation, is demonstrated.

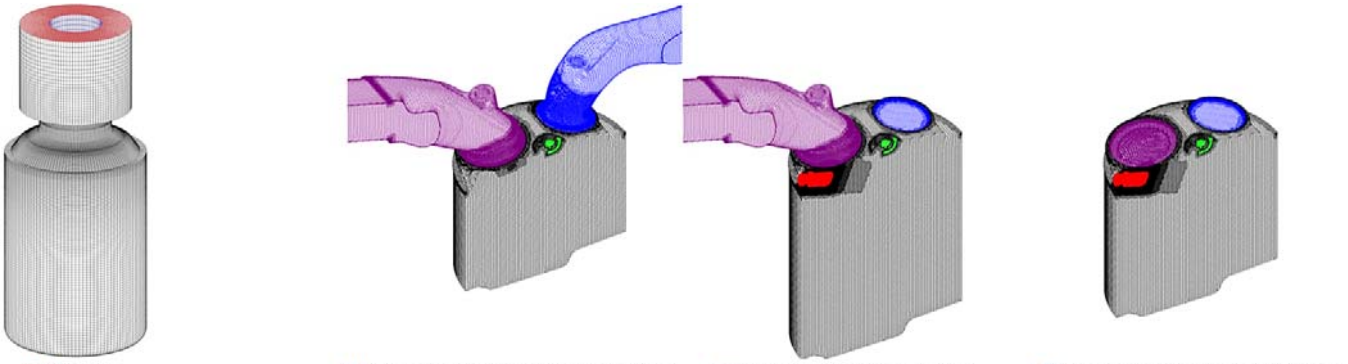

Figure 3. Computational grids: (a) injector grid, red – inlet pressure boundary, blue – moving needle valve; (b) (c) (d): examples of final engine grid at different stages throughout an engine cycle with or without the injector grid embedded depending on the injection timing, red – embedded injector grid

The pressure-based AVL FIRE code was utilized to solve the mass, momentum, and total energy conservation equations. The diffusive terms were discretized by the central differencing scheme and the convective fluxes by the second-order-accurate total-variation-diminishing (TVD) MINMOD scheme taking into account the expected appearance of shock waves in the underexpanded jet. The pressure-velocity coupling was solved by the SIMPLE algorithm. With respect to the turbulence modeling, despite the recent growing popularity of large-eddy simulation (LES) in engine-related studies, its application to high-velocity compressible gas jets still remains limited to basic academic cases. Therefore for the complete engine simulation with moving grids and gas injection in this work, the Reynolds-averaged Navier-Stokes (RANS) approach was adopted to have a reasonable computational time. In particular, the k-ζ-f formulation of the eddy-viscosity model was used, which is recommended for the applications with complex flow domain whereby the prerequisites for wall-nearest grid distance and grid uniformities can be relaxed while results in satisfactory agreement with experiments are still obtainable [26,27].

The reliability of the developed numerical model is methodologically compared with the outcomes of two recent mesh independence studies about gas injection in CNG engine with poppet-valve injectors similar to that in the current work [16,25]. Here the injector grid has 20 cells across the valve lift, which results in an average cell size less than 20 µm at the maximum valve lift and dwindling during transient phases. The choice of such grid resolution was based on the study presented in [25] arguing that 16 cells across the maximum lift of a poppet-valve type injector, with the first-order upwind scheme for the discretization of convective fluxes, would be sufficient to describe the distribution of fuel concentration and therefore the mixing process during injection. It was also pointed out that appreciable difference in describing the periodic structure of shock cells between the 16-cell resolution grid and a 32-cell one was observed, but the difference was localized in the near-field supersonic region, which is beyond the scope of the present study. Apart from the higher grid resolution, the numerical model here discretizes the convective fluxes using a second-order-accurate scheme instead of a first-order upwind scheme in [25], which further reduces numerical diffusion especially in the high-gradient region induced by the gas injection. In [16] the second-order-accurate MARS scheme was used for convective flux discretization but the finest mesh in the grid independence study for poppet-valve injector featured a cell size of 40 µm that is double the value in the present work. Moreover, the highest NPR here was below 16 whereas in both studies in literature the NPR was around 20. In conclusion, it is believed that the numerical model in this work is methodologically pertinent, especially in terms of grid resolution, to the intended study on air-fuel mixing process as a result of gas injection and the interaction thereof with engine in-cylinder flow. Further validation of the numerical model is provided by the comparison between planar LIF images and simulation results in the next section.

Results and Discussion

Results pertaining to the development of the CNG engine in three different aspects are presented and discussed in detail, namely (1) the implementation of the side-mounted direct gas injector regarding the considerations behind the injection angle choice specific to gas fuel application and the constraints on the injection operation; (2) the results about the thorough analysis of the gas injection and mixture formation process by means of planar LIF experiments and supplementary numerical simulations; (3) optimization results of the full-load performance of the prototype CNG engine in test bench with reference to the target power curve.

For the sake of clarity, crank angles in this work are all expressed by referring to the firing TDC as 720 or, cyclically, 0 degCA.

Injector Implementation

The results concerning the positioning and flow characterization of the direct gas injector are an essential prerequisite for the DI event design and mixture formation analysis, and are hence presented first in this subsection.

Apart from the advantages in available space for larger nozzle design and mechanical strength of the combustion chamber as mentioned in the engine overview section, the side-mounted injector configuration was preferred due to the fact that the injected fuel is in gaseous state and the potential interaction between the gas jet and intake-induced air flow in the combustion chamber can be exploited. In fact, the gaseous jet, unlike the liquid spray, issuing from a direct injector has relatively low momentum and limited penetration length, despite the high-velocity flow field characterizing the underexpanded jet [28]. Consequently, in the case of a centrally mounted injector, the rapid decline of axial momentum in the jet significantly hampers the jet impingement, especially for injection event occurring during intake or early compression stroke when the piston is too far away from the jet to exert any effective reflection. In most cases the fuel-air mixing process is dominated by free jet mixing, which can be observed for instance in [12,16,25].

On the basis of this observation, the side-mounted gas injector was adopted and the orientation was designed in such a way that the gas jet, on one hand, can be conveyed across the combustion chamber by the tumble flow generated during intake phase to overcome the low penetration, and on the other hand, can enhance the tumble flow by the momentum of the jet itself. Accordingly, the tumble-oriented injector configuration was realized by setting a quite flat angle of the injector axis. Furthermore, as schematically shown in Figure 4, a rough geometric estimation of the jet cone suggests that the injector niche would interfere with the jet and hence the actual jet would be further deflected towards the pent roof, aligning itself with the tumble flow formed by the intake air. The underlying principle of the jet deflection is the Coandă effect, the phenomenon of the formation of a low pressure zone between the high-velocity jet and adjacent approximately parallel surface as a result of the entrainment of surrounding fluid by the jet. The prospective occurrence of the Coandă effect, the extent to which the jet cone is deflected by it and the resultant flow characteristics has to be verified by the planar LIF experiments and the numerical simulations. It should be pointed out that such configuration was conceived with specific reference to the NG due to its intrinsic gaseous state without the risk of wall wetting, or evaporation issue.

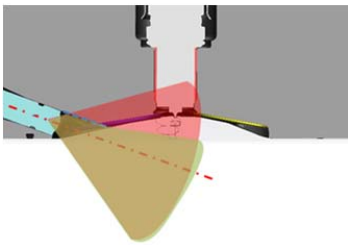

Figure 4. Estimated jet cones of the side-mounted injector: red – unaffected jet cone, green – jet cone intersected by injector niche

Characteristics of the injector impose certain constraints that have to be respected when devising the injection event. Firstly, precise fuel metering is instrumental to the engine operation which is commonly facilitated by imposing chocked flow in the injector nozzle. Choking enforces independence of the fuel mass flow rate from back pressure so that the injection rate can be prescribed by the rail pressure and temperature when the pressure in the combustion chamber varies continuously. Since the in-cylinder pressure rises rapidly during the compression stroke, and sonic flow condition in the nozzle throat for methane is guaranteed when the inverse NPR is less than 0.542, a limit to the latest possible end of injection (EOI) exists. Secondly, a secure closure of the injector tip prior to the start of combustion has to be ensured and therefore a safety margin of 2 ms is necessitated between the EOI and ignition event, which also constitutes a limit to the EOI. In particular, the maximum rail pressure of the CNG engine in this work is set at 16 bar, and taking into account the requirements concerning the sonic flow condition and the safety margin, the EOI limits at full load, for example, are reported in Figure 5. Values of the EOI limit for sonic flow indicate the crank angles where the pressure inside the combustion chamber approaches 8.5 bar. The specific values depend on the boost level and the intake valve actuation at each operating point and were estimated by a one-dimensional engine model with GT-Power, whereas the SA values were empirically derived from existing CNG engines. It is noted that above 4500 rpm the limiting factor for the latest EOI is the safety margin, whereas the elevating back pressure during the compression stroke becomes critical at lower engine speeds. Also, should further postponing the EOI limit be the purpose, increasing the rail pressure will result in feeble improvement as the gap between the two constraints is small, especially at engine speed above 3000 rpm.

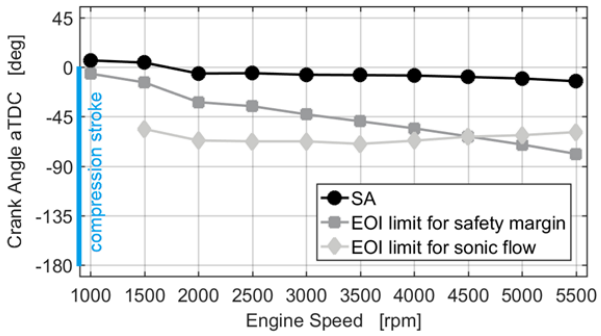

Figure 5. Limits on the EOI for full-load operating points and rail pressure 16 bar (the ordinate is expressed in degCA after the firing TDC)

Another constraint of the injector characteristics, depending on the engine operating points, is imposed on the rail pressure at which the fuel is injected. When the requested fuel quantity is large, e.g. at rated power, the rail pressure should be kept at the maximum value to curtail the total injection duration so that the injection window can stay within the allowable range of timing and maintains the flexibility of being postponed relative to the IVC for volumetric efficiency gain, if necessary. On the contrary, when the requested amount of fuel considerably reduces, e.g. at idle or low load, the injection duration should be prolonged by lowering the rail pressure so as to prevent the injector from working mainly, if not completely, in the non-linear transient flow-rate zone (i.e. closing the valve during or shortly after the opening), and to thus avoid irregularity caused by the unstable injection flow rate. For this reason, being 16 bar the maximum value, a variable rail pressure strategy was employed whereby the pressure level could be decreased below 16 bar through an electronic pressure regulator mounted upstream of the fuel rail.

The injected fuel quantity and the corresponding injection duration at different rail pressure levels was tested, as shown in Figure 6 wherein only the linear operating range of the injector is reported since the aforementioned non-linear transient flow-rate zone due to further shorter injection duration should be avoided. It is verified, first of all, that the maximum rail pressure of 16 bar is sufficient to deliver the requested fuel quantity for all the full-load engine operating points while reasonable injection duration is warranted within the allowable timing limit. Then the characterization results are used to determine the injection duration for each individual engine operating point according to the requested amount of fuel.

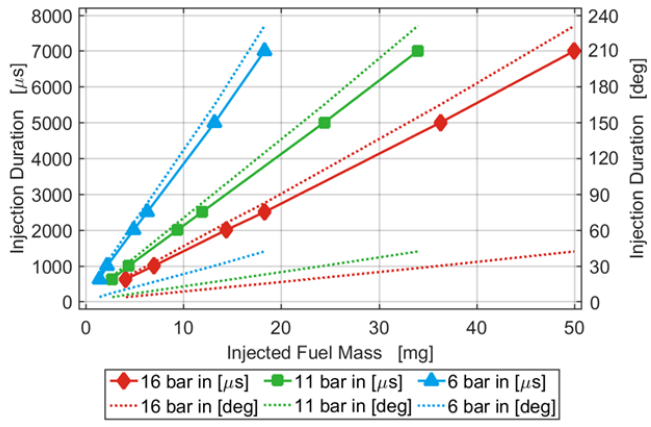

Figure 6. Rig-test results of the injected fuel quantity and corresponding injection duration at three different pressure levels: each pair of dotted lines –

injection duration at 5500 rpm (upper) and 1000 rpm (lower)

In summary, the characterization of the gas injector reveals two prerequisites that circumscribed the design of DI operation, namely the limits on EOI and the injection duration-quantity characteristics at variable rail pressure. The former was used to fix the injection timing and the latter the injection duration, which in combination constitute the guideline for devising injection events over the entire engine map.

Gas Injection and Mixture Formation Process

This subsection is dedicated to the results from an extensive analysis, experimental and numerical, of the DI and mixture formation process in the combustion chamber with side-mounted direct gas injector. Also, interaction of the gas jet with intake-induced air flow and geometrical bounding walls as well as the turbulence evolution inside the combustion chamber was investigated in detail. All these aspects combined together allowed a deep and sound understanding of the underlying fluid-dynamic characteristics that influence the mixing process between air and fuel, which in turn, affects efficiency of the homogeneous stoichiometric combustion and emissions. It should be noted that, as described in experimental setup section, the LIF result at each crank angle is the corrected and averaged image, over 35 repetitions, in the same symmetry plane of the combustion chamber. Also, for later crank angle higher uniform multiplier was applied to augment the otherwise declining maximum light intensity as the mixture homogenized, which was suitable to facilitate recognition of the mixture pattern within each single image. The images are all in grayscale corresponding to the captured fluorescence intensity, with the brighter color representing higher intensity.

In particular, three engine operating points were investigated, namely the low-end torque 1500 rpm full-load point, a low-speed 2000 rpm part-load point, and a high-speed 5500 rpm full-load point, each with distinct features worth being examined.

Firstly, the 1500 rpm full-load point was considered. In this case, the very late injection, with SOI just after IVC as shown in Figure 7, was solely of practical interest as it was anticipated that the low-end target torque had to be obtained by maximizing the volumetric efficiency and therefore the gaseous fuel displacing fresh air during intake phase avoided. However, the low-end torque point is well known as the most critical point in regard to charge motion and hence the air-fuel mixing capability because of the low piston speed yet high torque-delivering request. The very late injection timing made the situation even more problematic due to the unfavorable mixing time left.

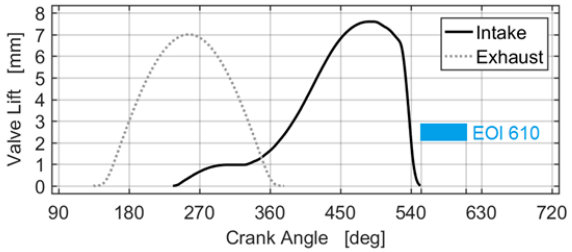

Figure 7. Injection timing and corresponding duration: 1500 rpm full-load

For this reason, the investigation at the 1500 rpm full-load point was concentrated on the quality of mixture formation and the mechanisms thereof. The results from planar LIF and numerical simulations are presented in Figure 8 wherein, and in all the other similar figures, the LIF results are obtained in the laser-illuminated plane (the symmetry plane) whereas the numerical simulation results represented in three mutually perpendicular planes – the symmetry plane as well as the horizontal plane coincident with the cylinder head gasket (called gasket plane hereafter) and a vertical plane on the intake side passing though the near-downstream of the injector nozzle exit (called intake-side plane hereafter).

It can be observed in the LIF image at 570 degCA (Figure 8a) that the Coandă effect manifests itself immediately after SOI as the jet is deflected to the pent roof instead of proceeding along the injector axis to form a hollow cone. The jet continues being forced by the Coandă effect to remain attached to the pent roof from the intake side up to the exhaust side where the jet is then redirected downwards to the piston as shown by the LIF image at 610 degCA (Figure 8b). When viewed in the laser-illuminated symmetry plane, the entire course of the fuel-rich cloud established by the injection follows the primary tumble motion, clockwise in this case, typical of gasoline-like engine with pent roof. Given the risk of ignition by the laser energy when thermodynamic state of the mixture was too high, the last LIF image was acquired at 670 degCA (Figure 8c) wherein exists a modest degree of mixture inhomogeneity with the mixture on the intake side being slightly richer than the exhaust side.

On the basis of the experimental observations above, effectiveness of the side-mounted injector orientation is confirmed as far as the Coandă effect and the reinforced jet penetration by tumble flow transport is concerned. The air-fuel mixing process, nevertheless, seems to be limited by the fact that the rich cloud follows, and is restricted within, the clockwise tumble motion attaching to the cylinder walls with rather limited mixing with the air across the bulk region of the combustion chamber. In the subsequent combustion measurement, the IMEP reaches the target value and the coefficient of variation (CoV) of the IMEP measures less than 1.2%, indicating that, despite the inhomogeneity seen in the last LIF image, the mixture quality is good enough for an efficient combustion.

Fuel distribution results from the corresponding numerical simulation at the same crank angles as the LIF images are shown for comparison (Figure 8d, e, and f). The simulation results in the symmetry plane, especially the jet evolution and redirection of the rich cloud on the exhaust side liner, are in quite good agreement with the LIF images, indicating that the developed numerical engine model is of reliable predictability. It has to be pointed out that the injector niche, as recessed in, and therefore blocked by, the combustion chamber roof, is not visible in the LIF images.

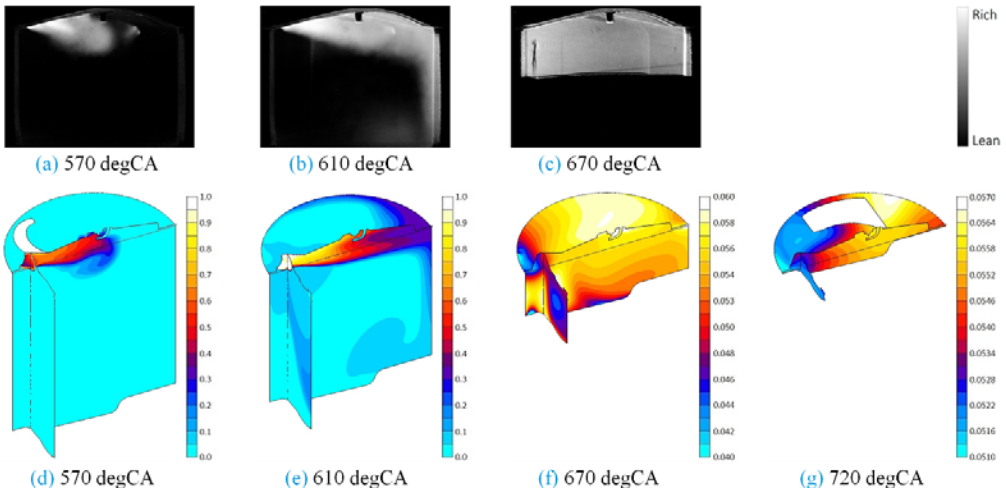

Figure 8. Planar LIF images and fuel concentration contours at selected crank angles: 1500 rpm full-load, LIF – in grayscale, numerical model – in color

Supplementary to the experimental measurement, additional insight into the air-fuel mixing process is disclosed by the numerical model. Upon reaching the exhaust side in alignment with the tumble motion (Figure 8e), the rich cloud is, on one hand, redirected vertically downwards following the tumble flow pattern as confirmed by the LIF measurement, and on the other hand, reflected tangentially sideward into a swirl-like motion as shown in the gasket plane. Furthermore, as can be perceived from the concentration contours, the amount of fuel involved in the swirl motion is comparable with, or even larger than, that in the tumble motion. Moreover, in the same crank angle it is observed that the transport speed of the swirl motion is higher, as the rich cloud front has already circulated back to the intake side (as shown in the intake-side plane). The reason is assumed to be that the circular path followed by the tangential swirl motion is more flow-favorable than the rectangular path of the tumble motion. Considering moreover the symmetric existence of two swirls on both sides, the ellipse-shaped swirl motion, traveling from the redirection point in the exhaust upper corner to the intake lower corner, is rather beneficial to the air-fuel mixing process, in addition to the intended tumble motion. Given this additional insight, the tumble motion pattern of the rich cloud, seen in the symmetry-plane LIF images, is partially the homogenization mechanism that is in fact largely augmented by the elliptical swirl flow and turns out to be very effective.

Without the practical constraint of experiments, the mixing process is shown by the numerical simulation beyond the last LIF image. While the modest inhomogeneity with richer mixture on the intake side at 670 degCA is well reproduced by the numerical model (Figure 8f), the mixture quality has noticeably improved during the remaining 50 degCA till the ignition event around the firing TDC (Figure 8g), accounting for the subsequent efficient combustion process.

Additional fluid-dynamic information relevant to the injection event is further derived from the numerical simulations and reported in Figure 9 wherein CoV and F_f refer to the coefficient of variation of the local fuel concentration across the combustion chamber and the flammability fraction, respectively, both of which are introduced as quantification indices of the air-fuel mixing process. Flammability fraction is given by the following expression:

$$F_f = \frac{mass\ of\ fuel\ included\ in\ the\ flammable\ mixture}{total\ mass\ of\ fuel} \quad (2)$$

With respect to the simulation results, the mass of fuel included in the flammable mixture is evaluated by summing up the mass of fuel in all the computational cells whose cell-wise relative air-fuel ratio is between 0.7 and 1.7, the flammable range of methane established according to available experimental data on CNG engines [29, 30]. The tumble motion is quantified by the dimensionless tumble number, relative to the instantaneous volume center of the cylinder, which is given by the following expression:

$$Tumble\ Number = \frac{\sum m_i[w_i(X_i - X_V) - u_i(Z_i - Z_V)]}{\frac{2\pi N}{60}\sum m_i[(X_i - X_V)^2 + (Z_i - Z_V)^2]} \quad (3)$$

where,
m_i = mass of the cell i [mg]
X_i, Z_i = x- and z-coordinates of the computational cell i [mm]
X_V, Z_V = x- and z-coordinates of the cylinder volume center [mm]
u_i, w_i = x- and z-component of the velocity of the cell i [m/s]
N = engine speed [rpm]

As shown in Figure 9, obvious intensification of the tumble motion and turbulence during the injection event is observed as expected from the flat injector orientation and high-velocity gas jet. Further discussion about the tumble and turbulence is given in the subsequent cases when multiple injection timings are compared. In spite of the anticipated low charge motion at low-end speed, the air-fuel mixing rate is impressive as demonstrated by the slope of the declining CoV curve. In particular, the mixing rate is substantial during the injection event and then considerably slows down after the EOI, which constitutes the first evidence that the mixing process is dominated by the gas jet during injection and flow patterns promoted by it, i.e. the tumble and elliptical swirl motion. Furthermore, the mixing rate decreases already shortly prior to the EOI, suggesting the abatement of jet-promoted motion as the injector valve closing reduces the momentum introduced by the gas jet.

In addition, the momentary increase in the mixing rate immediately after the EOI is likely attributable to the strong dilution of the trail of the jet-promoted motion that previously attached to the pent roof due to the Coandă effect and was continuously supplied by the injection with restricted bulk mixing with surrounding air as observed for instance by LIF experiment in the case of the aforementioned rich cloud following the tumble motion. In fact, while the CoV index quantifies the overall homogeneity of the whole mixture, the F_f index

distinguishes the mixture composition inside and outside the flammable range. Specific to the time instant under question, the momentary increase in mixing rate corresponds to a remarkable increase in the flammable fraction, implying that a drastic re-composition occurs at the rich or lean end. The abovementioned trail dilution seems to be a plausible explanation since the appearance of the rich trail due to ceased injection supplying is the only change shortly before and after EOI. Finally, the F_f curve shows that, while the mixture homogeneity is still slowly improving, the whole mixture has been within the flammable range well ahead of ignition at firing TDC, accounting for the efficient combustion process.

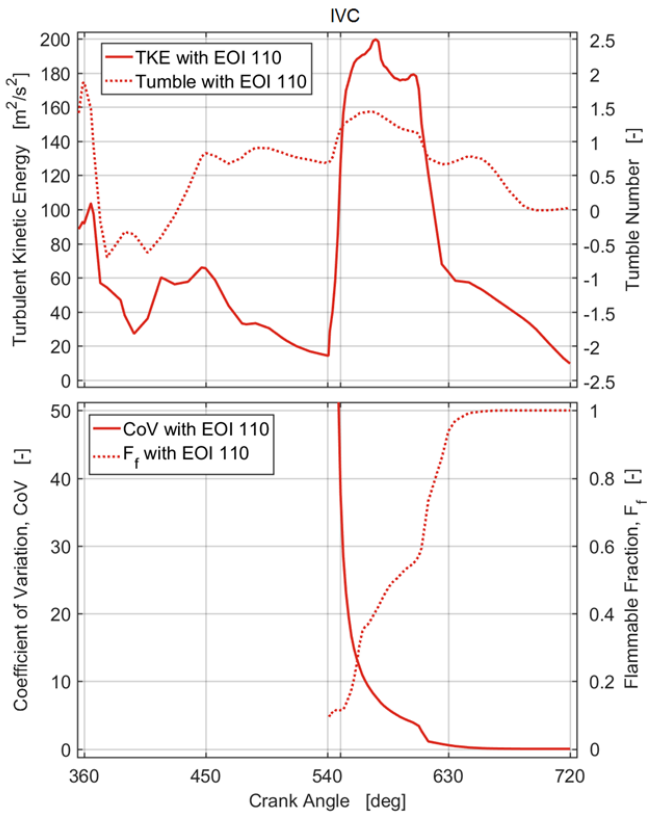

Figure 9. Temporal evolution of turbulence, tumble flow, and mixing process inside the combustion chamber: 1500 rpm full-load

Secondly, the 2000 rpm part-load (IMEP 4 bar) point was examined for the reason of its sensitivity to mixture homogeneity. From engine operation point of view, the low-load operating points are commonly optimized for fuel consumption and therefore work with early IVC (EIVC) which inevitably compromises the intake-induced charge motion and, consequently, deteriorates the mixing capability and turbulence level to the extent near the combustion stability limit. Accordingly, three injection timings with distinct implications were identified, as shown in Figure 10, wherein the significantly reduced intake valve actuation and extreme EIVC is noted. Starting from a very late injection close to the EOI limit and fully completed after IVC, the injection event was advanced to an intermediate timing partially before IVC, and then further advanced to a very early timing when the injection occurs during intake phase and is hence very similar to a PFI situation.

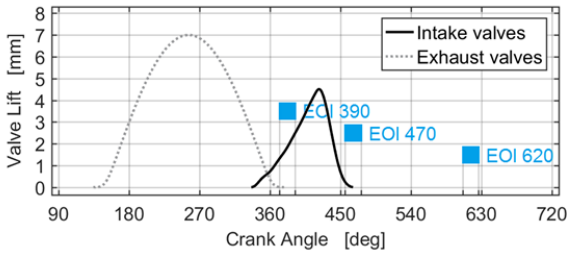

Figure 10. Injection timings and corresponding duration: 2000 rpm part-load

The results from planar LIF and numerical simulations are presented in Figure 11. Since the simulation results, like in the case of 1500 rpm full-load point, are in good accord with the LIF images in the symmetry plane, here the case-by-case comparison is omitted and the simulation results are presented as supplementary perspective to LIF experiment where necessary. The other fluid-dynamic quantities from the numerical simulations are reported in Figure 12.

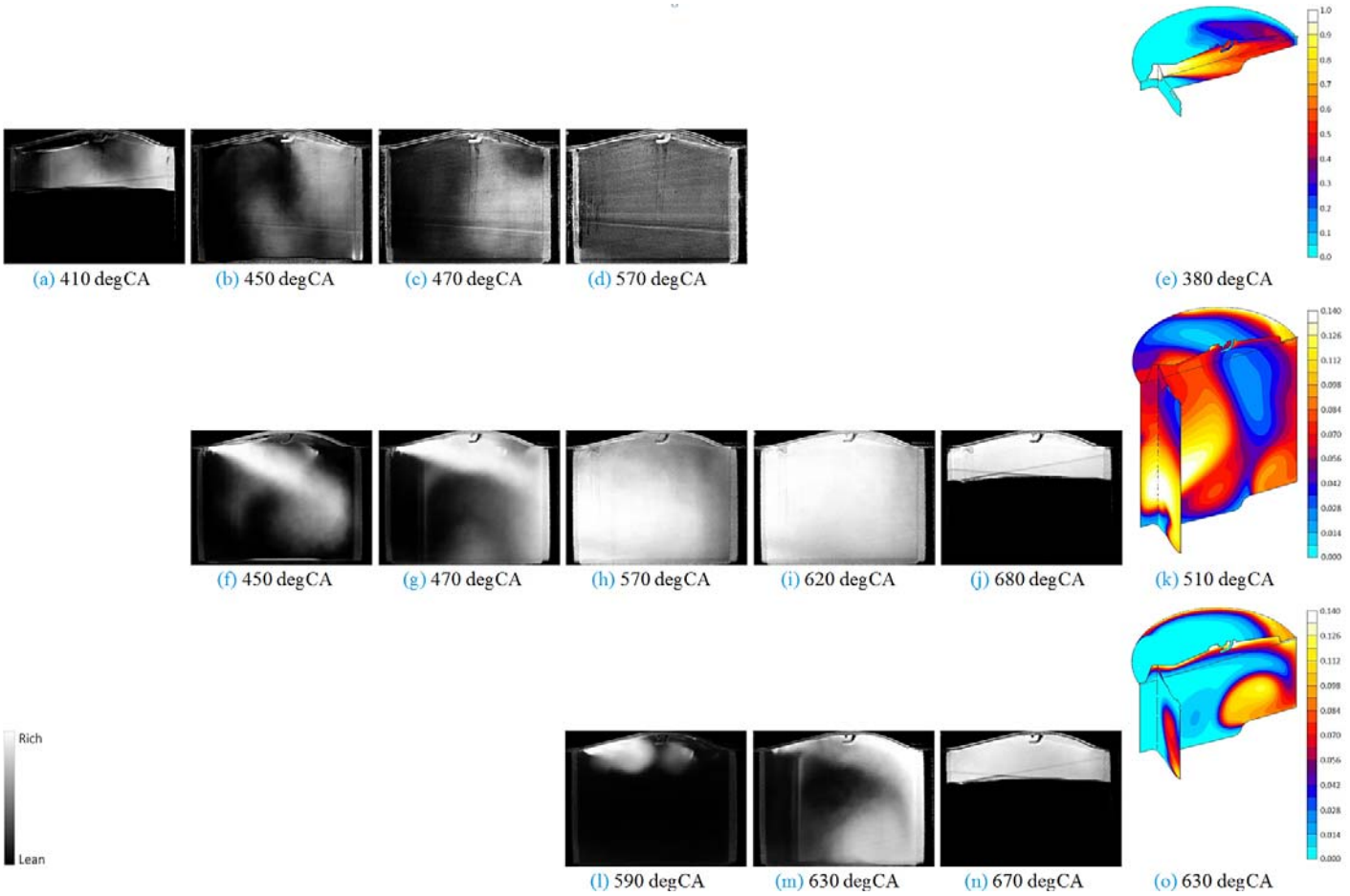

Figure 11. Planar LIF images and fuel concentration contours at selected crank angles: 2000 rpm part-load, LIF – in grayscale, numerical model – in color, first row (a) – (e) EOI = 390 degCA; second row (f) – (k) EOI = 470 degCA; third row (l) – (o) EOI = 620 degCA

Due to the different injection timings relative to the intake phase, the jet interacts with the intake air flow in different ways which lead to distinct jet evolution and mixing behaviors. As for the early injection event (EOI = 390) which is very close to the valve overlapping TDC, no image was acquired during the injection because the available space for laser sheet access was insufficient for reliable LIF response. Subsequent LIF images (Figure 11a, b, and c) indicate that the fuel-rich cloud moves in the anticlockwise direction, i.e. the inverse tumble, contrary to the clockwise tumble that should typically be the primary intake air motion. The reason is that the intake phase is heavily reduced by the relatively low intake valve lift and extreme EIVC, and more importantly, that the piston crown shape favors the anticlockwise flow motion when moving downwards. Consequently, when the intake air flow is not strong enough, the overall flow will be dominated by the inverse tumble formed by the piston movement. It is confirmed by the tumble number evolution (see Figure 12) since, except for the ongoing injection periods, the tumble number of all the three injection timings is majorly negative. As a matter of fact, even in the full-load case where the intake valve actuation is enlarged the tendency of inverse tumble formation due to the piston downward movement is still evident in the first half of intake stroke (See Figure 9). The inverse tumble is most obvious in the early injection case since, on one hand, the jet is constantly affected by the intake air flow that inhibits the Coandă effect, and on the other, the piston crown guides the impinged jet in the anticlockwise direction in alignment with the inverse tumble as revealed by the simulation result (Figure 11e). Consequently the whole engine cycle is featured by the inverse tumble with the injection event further intensifying it, which explains the observation in LIF images. With respect to the mixing process, substantial mixing rate is found during injection which is similar to the behavior of 1500 rpm full-load case. However, the underlying mechanisms responsible for the mixing process are disparate. In this case the mixing is attributable to the jet-piston impingement without noticeable transport of fuel by tumble or swirl motion. Moreover, it is noted that the F_f curve rises slower, also with a delay, in comparison with the decline of the CoV curve. Actually, even though the mixing process is greatly expedited by piston reflection, i.e. the fast decline of the CoV curve, the injection is completed within a small portion of the intake phase and therefore the overall mixture composition is still beyond the rich end of the flammable range, i.e. little variation of F_f curve. This also explains the small fluctuation of the CoV curve after the major decline, being the increase in fresh air during the remaining intake phase. Given the effective mixing through jet-piston interaction and the ample mixing time, the mixture is quite homogeneous, entirely within the flammable range more than 100 degCA ahead of the ignition event (See Figure 11d and Figure 12).

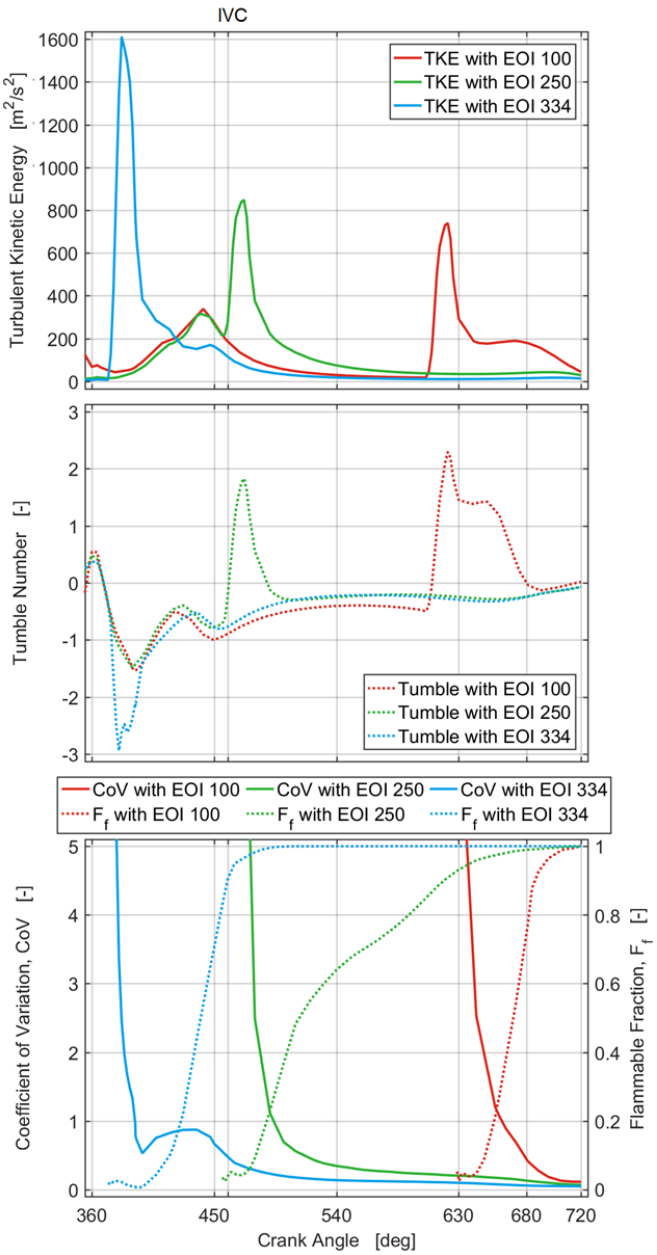

Figure 12. Temporal evolution of turbulence, tumble flow, and mixing process inside the combustion chamber: 2000 rpm part-load

For the intermediate injection case (EOI = 470 degCA), the injection is started when the strong intake air flow has been initialized by the relatively wide-open intake valves and suction force from the piston. The intake air impedes immediate formation of the Coandă effect and in consequence the hollow cone jet is allowed to develop along the geometrical injection axis. But as IVC precedes EOI, during the ongoing injection after IVC the Coandă effect comes into effect whereby the jet is directed to the pent roof and the tumble motion of rich cloud established (see Figure 11f and g). The LIF images at 570 and 620 degCA (Figure 11h and i) are featured by a rich cloud appearing in the intake lower corner, which, according to the simulation result (Figure 11k), is not related to the tumble motion but to the elliptical swirl transporting the fuel from the exhaust upper corner to the intake lower corner along its elliptical path.

The late injection case (EOI = 620 degCA) is critical both for the much reduced available mixing time and for the weakened charge motion by the time of SOI due to very EIVC. The LIF images (Figure 11l and m) confirm that the Coandă effect, when undisturbed by the intake air flow, forces the gas jet to attach to the pent roof right after SOI and to follow the tumble motion. The numerical result at the same crank angle (Figure 11o), showing the faithful prediction of fuel distribution of the LIF image in the symmetry plane, underlines formation of the elliptical swirl accompanying the tumble motion.

The mixing mechanism for the intermediate and late injection cases, disclosed by the simulation results, is consistent with the findings in the 1500 rpm full-load case. The difference between the two part-load cases is the strength of the jet-promoted tumble and swirl motion. Since in the intermediate injection case the gas jet is initially deviated from the tumble motion, the fuel conveyed in the tumble is less than that in the late injection case and the tumble motion is less promoted by the jet momentum. Indeed, the simulation result of the intermediate injection case (Figure 11k) shows that the amount of fuel involved in the tumble is much less than that by the elliptical swirl, whereas such discrepancy is not evident in the late injection case (Figure 11o). As it is concluded previously that the mixing process in this situation depends on the combinative effect of the jet-promoted tumble and swirl motion, the lower mixing rate of the intermediate injection case (see Figure 12) substantiates the less effective mixing process due to the weaker tumble peak induced by the event of injection. Besides, the much slower increase in the flammable fraction indicates the lack of mixing site that is most likely ascribable to the lower amount of fuel involved in the tumble motion as well.

From the evolution of tumble numbers in Figure 12, it is firstly seen that the tumble motion is so largely intensified by the jet momentum as to predominate over the negative one formed by the piston to have an overall positive tumble number during the, albeit short, injection periods. Secondly and more importantly, that the so short appearance of jet-promoted tumble, and accompanying swirl motion, is responsible for the majority of CoV decline, i.e. homogenization, constitutes the second evidence that the mixing process is dominated by the gas jet during injection and flow patterns promoted by it. This is especially evident for the late injection case in which development of the jet-promoted flow patterns, and therefore effectiveness of the mixing mechanism, is guaranteed the most. Moreover, comparing CoV and F_f curves between the early and late injection implies that the mixing mechanism of tumble and swirl transport is comparable with direct jet-piston impingement in terms of mixing capability.

Despite the unfavorable mixing process, LIF image (Figure 11j) shows that the intermediate injection timing is still early enough to achieve homogeneous mixture. And due to the high mixing rate of the late injection, even though the last LIF image at 670 degCA (Figure 11n) shows richer intake side and leaner exhaust side, the mixture is in fact of good homogeneity shortly afterwards. In terms of the final mixture quality, all three injection timings result in almost identical flammability fraction and mixture homogeneity, with the late injection timing (EOI = 620 degCA) having slightly higher CoV at the ignition event. In this regard, it is also confirmed that such VVA profile of extreme EIVC at this operating point, albeit significantly altering the coherent flow structure in comparison with full-load case, guarantees adequate mixture quality while fulfilling the optimization of volumetric efficiency, thanks to the mixing mechanism introduced by the side-mounted injector.

Experimental measurements of the combustion stability and rate for the three injection timings are reported in Table 1 wherein SA is expressed as degCA before firing TDC and the burning rate relative to the firing TDC as 0 degCA. The MFB50 was set to 8 degCA that resulted in the maximum efficiency for all the three cases.

Table 1. Combustion stability and rate: 2000 rpm part-load

Timing	**SA** [deg BTDC]	**CoV** IMEP	**Burning Rate**		
			MFB5 [degCA]	**MFB50** [degCA]	**MFB90** [degCA]
Early	27	3.0 %	-8	8	22
Intermed.	18	2.4 %	-4	7	16
Late	14	1.9 %	-2	8	15

The first phase of combustion, which can be considered as the period between SA and MFB5, is appreciably longer as the injection is advanced. The combustion duration, given by the time between MFB5 and MFB90, exhibits the same trend. Also the combustion stability increases with delaying injection timing. According to the mixture quality analysis above, it is clear that the flame kernel development and flame front propagation is mainly determined by turbulence level in the combustion chamber.

Difference in the turbulence level is connected with the different injection timings since the engine operation parameters are otherwise the same for all the three cases. The gas jet enhances the turbulence level in a twofold fashion – intensifying the large-scale motion and introducing small-scale vortices in the shear stress area around the high-velocity jet – which disintegrates and transforms into smaller eddies amounting to the increase in turbulence level. With reference to the evolution of turbulent kinetic energy in Figure 12, the steep increase in turbulence at each SOI is mainly attributable to the small-scale vortices. Such increase is the largest for the early injection due to the piston-impingement, moderate for the intermediate timing due to the interaction between jet and intake air, and the smallest for the late timing since there is no extra effect other than the shear stress between the high-velocity jet and low-velocity air. However, turbulence level diminishes rapidly at EOI as the small-scale vortices are all too easily dissipated over time. It is the jet-intensified large-scale charge motion that carries more kinetic energy for later turbulence production. In fact, although the peak turbulence of the early injection is the highest, it drops below the level of the late injection just before SOI of the latter, since the inverse tumble intensified by the early injection jet is in contradiction with the intake-induced tumble and thus the resultant net charge motion that persists throughout the compression stroke remains low.

Therefore, later injection benefits more from the turbulence created by itself, as tumble flow is intensified by the jet being not disrupted by the intake air, is less dissipated before the ignition event and therefore energizes more turbulence. This is evidenced by the late injection case wherein, as shown in Figure 12, the small increase in turbulence kinetic energy at about 680 degCA after the rapid decline, and the corresponding decrease in tumble number, indicates the production of turbulence by the jet-promoted tumble flow. This characteristic of gaseous fuel injection is remarkably unique since in conventional GDI engines the turbulence mainly originates from intake air-induced charge motion and not much from charge motion promoted by liquid fuel spray.

Thirdly, the 5500 rpm full-load point was examined as the ample intake window and high piston speed would generate potent intake-induced charge motion that interacted with the gas jet in a different way than the mechanisms previously seen. Moreover, the injection duration was inevitably long in terms of crank angles due to the large fuel quantity requested and more importantly, the high engine speed. As shown in Figure 13, three injection timings were identified which, due to the long injection duration and intake VVA with IVC extended up to mid-compression stroke, were all similarly confined within the intake phase, albeit in slightly different stages.

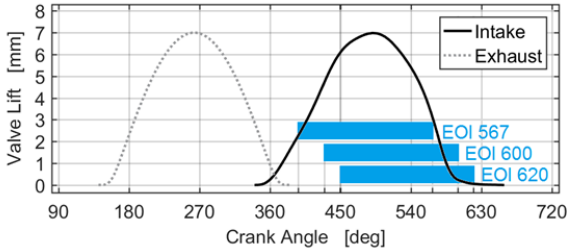

Figure 13. Injection timings and corresponding duration: 5500 rpm full-load

This operating point is investigated with the numerical model since the engine speed exceeds the allowable speed limit by the glass liner of optical engine. The simulation results of the intermediate timing (EOI = 600) are presented in Figure 14, representative of all the three timings due to their similitude. Since the entire injection event occurs during the intake phase, the gas jet is constantly being deflected by the intake air flow while the Coandă effect opposite to it is restricted (see Figure 14a). Therefore, the jet is not redirected to the exhaust upper corner and the formation of the elliptical swirl motion observed in the 1500 rpm full-load case is suppressed. Nevertheless, the jet is still effectively transported by the tumble motion that is particularly substantial in this case. Subsequently, when the intake valve lift reduces, the Coandă effect predominates to deflect the jet upwards to the pent roof and the jet-promoted near-wall tumble and swirl motion is established. Result at 10 degCA after EOI (Figure 14b) shows that the rich cloud front conveyed by the tumble motion has already circulated back to the intake side while the swirl motion is relatively weak, which is exactly the opposite of what is observed in the low-speed full-load case.

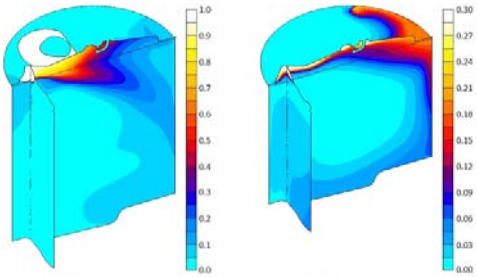

Figure 14. Fuel concentration contours at selected crank angles: 5500 rpm full-load, EOI = 600 degCA

The relevant fluid-dynamic quantities are reported in Figure 15. First, the inverse tumble with negative tumble number formed by the piston crown close to TDC is recognized also in this case. Then the strong intake-induced tumble, together with the gas jet, dominates the whole flow field with the tumbling motion that accounts for the effective transport of rich cloud, unseen in the previous cases. Moreover, the tumble remains at a quite high level because it is constantly sustained

thanks to the late IVC and long injection duration. With respect to turbulence, a noteworthy increase in the turbulence level shortly before the firing TDC implies the dissipation of high-kinetic energy large-scale flow and hence the existence of the high-velocity tumble motion. In summary, owing to the similarity of the three injection timings and the contribution of the potent intake-induced flow to the formation of a predominant tumble motion, the turbulence level at the ignition event near the firing TDC resulting from the three injection timings is not distinctive enough to affect the combustion process in different ways.

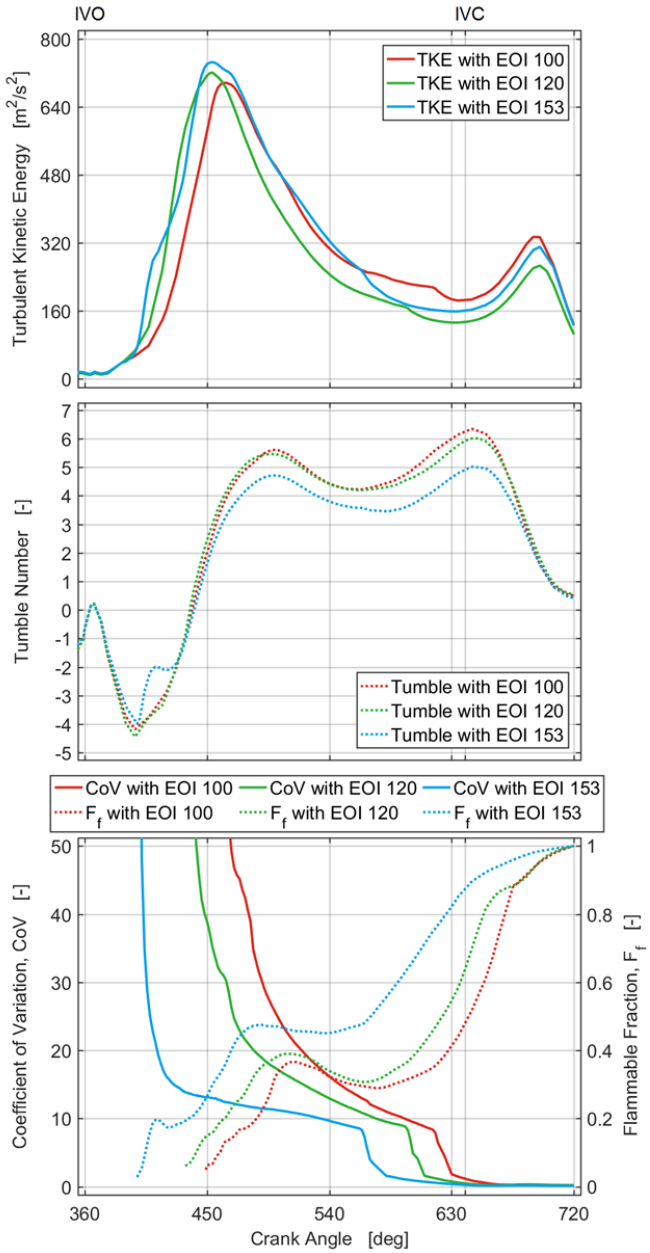

Figure 15. Temporal evolution of turbulence, tumble flow, and mixing process inside the combustion chamber: 5500 rpm full-load.

As far as mixture quality is concerned, at the ignition event the three injection timings are equivalent in terms of both flammable faction and homogeneity. However, the converging trends of the CoV curves and F_f curves, i.e. the later injection event having higher mixing rate, indicate that the mixture formation process is different. In fact, on the basis of the previous observation about Figure 14, later injection is featured by earlier appearance of the Coandă effect relative to its injection duration and thus has longer time for the development of jet-promoted tumble and swirl motion. Specific to the current case, the difference in jet-promoted tumble motion is overshadowed by the reinforcing contribution of the strong intake air flow. Nevertheless, the tumble number evolution still shows some difference among the three injection timings, being that later injection leads to higher tumble number starting from its individual SOI.

Trends of the CoV curves of the intermediate and late injection in this case are rather similar to that of the 1500 rpm full-load case, since the high-speed cases have very similar EOI to the low-speed one and, despite their difference in the relative strength of tumble and elliptical swirl, they share the same mixing mechanism that is the jet-promoted motion. However, the mixing rate in crank angle degrees in the low-speed full-load case is much higher. Should the mixing process depend on air charge motion, the mixing rate will correlate with the engine speed, i.e. the high-speed cases should have the same mixing rate in crank angles as the low-speed one. Indeed, considering the implication of different engine speeds, the mixing rates of the two 5500 rpm full-load cases in absolute time are slightly higher than the 1500 rpm full-load case. This is expected as in the high-speed case the jet-promoted tumble is combined with potent intake-induced flow to form a quite substantial tumble motion, which partially enhances the mixing mechanism. The observation that the mixing rate correlates with absolute time rather than engine speed constitutes the third evidence that the mixing process is dominated by the gas jet during injection and flow patterns promoted by it. Furthermore, the trail dilution, the momentary increase in mixing rate immediately after EOI, previously observed in the 1500 rpm full-load case is also present for all the three 5500 rpm full-load cases.

Power Curve Optimization

Based upon the outcome of the specific implementation of the gas injector and of the mixture formation analysis in the combustion chamber, a multi-cylinder prototype engine is built for optimization test. The objective, as stated in the engine overview section, is to achieve the same rated torque and power of the boosted GDI version from which the CNG engine combustion chamber has been derived, starting from the power curve of an existing PFI CNG engine as reference and eventually aiming to improve the overall appealing of CNG engines and vehicles to end customers.

The final achievement of the target power curve was divided into multiple stages whereby the roadmap of contributions ascribable to various improving factors could be identified. Figure 16 describes the resultant power curve of each stage of improvement.

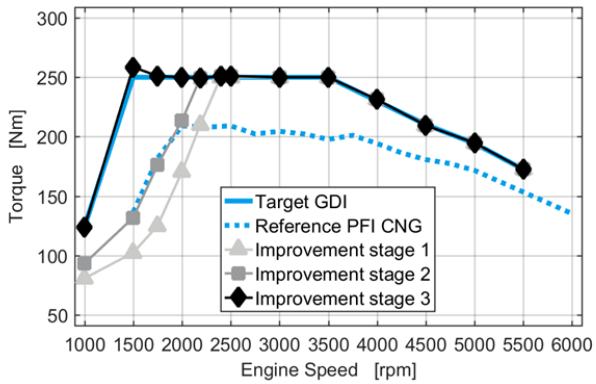

Figure 16. Optimization of power curve on the prototype engine

The first stage of improvement in comparison with the reference PFI engine consisted in a properly sized turbocharger for the engine in question together with the EIVC strategy for optimizing volumetric efficiency, which fulfilled the performance target above 2500 rpm. Due to the elevated CR and advanced SA specifically devised for NG, however, the exhaust temperature reduced as a result of higher engine internal efficiency and advanced combustion, which in turn decreased the enthalpy delivered to the downstream turbine and the performance thereof at low speed. So the low-speed power curve lies below the reference one. However, the attainment of the highest possible low-end torque is of primary importance, as it warrants prompt acceleration maneuvers. Also a higher gear ratio can be accordingly adopted, being beneficial to fuel consumption. Introducing cooling effect of the underexpanded jet during intake phase in attempt to increase volumetric efficiency proves counterproductive since the injected gaseous fuel occupying the volume, which should have otherwise been available for fresh air, overshadows any benefit of charge cooling. Instead it was found very advantageous to postpone the complete injection event after IVC to free up the space for fresh air. According to the mixture formation analyses at the 1500 rpm full-load point, the mixing mechanism due to the injector and combustion design allows homogeneous mixture to be obtained with such late injection timing. Also the CoV and F_f curves in Figure 9 indicate the margin for even later injection as far as the EOI limit required by the injector is not exceeded. Therefore, by fixing the EOI to the investigated value or slightly later, this strategy as the second stage of improvement was executed to allocate the injection event completely (at low speed) or mainly (at medium speed) after IVC. However, this enabling factor for improvement in volumetric efficiency is unattainable for high-speed operating points as the injection duration is too long. The loss of volumetric efficiency owing to the unavoidable part of fuel injection ahead of IVC at high engine speed was compensated by adopting slight higher boost level than in the GDI engine, since the enthalpy delivered to turbine is sufficient in this case.

The remaining low-end performance gap was bridged by adopting an innovative VVA design with a particular feature, enabled at low engine speed, which realized an intake valve pre-lift prior to the normal IVO (see Figure 7). Basically the intake valves are partially opened in the later exhaust discharge phase so as to enable a strong scavenging that considerably increases the volumetric efficiency. To retain the effectiveness of scavenging, very late injection timing is necessitated and the applicability is again confirmed by the mixture formation analysis. After the implementation of the third stage of improvement, the target GDI power curve was fulfilled by the DI CNG engine.

Conclusions

For the purpose of developing a mono-fuel small-displacement turbocharged CNG SI engine equipped with advanced VVA system and side-mounted direct gas injector, the present work has focused on the analysis of the combustion system design from the perspective of gas injection and mixture formation that is dependent on the gas injector implementation and VVA profiles.

Taking into account the challenging task of mixture preparation for homogeneous stoichiometric combustion with DI of NG, the side-mounted tumble-oriented injector configuration has been adopted to overcome the typical penetration problem of gas jet. The design of a flat injection angle with injector niche interfering with the jet cone, to exploit the Coandă effect, is verified to be efficacious. Considering the constraints of sonic flow condition and safe closure of the injector tip, the EOI limits were established. Moreover, due to the request of variable rail pressure for engine operation, the flow characterization of the injector was tested with respect to injected fuel quantity and corresponding injection duration. The EOI limits and the injection quantity-duration characteristics are useful for fixing the injection timing and duration, respectively, and constitute the guideline on injection window design for all engine operating points.

The gas injection, the interaction thereof with intake-induced charge motion and geometrical bounding walls, and the resultant mixture formation process was experimentally and numerically investigated in detail, in order to verify the design of combustion chamber and injector. In particular, three representative engine operating points were analyzed through which it was found that the mixing process is dominated by the gas jet during injection and flow patterns promoted by it. In general, the principal mixing mechanism is the jet-promoted motion patterns, namely the tumble and elliptical swirl motion. Specifically, the Coandă effect forces the high-velocity jet to attach to the pent roof up to the exhaust upper corner where the jet is then redirected downwards, forming the tumble, and sideward, forming two symmetric swirls. The air-fuel mixing rate is mainly determined by the strength of the two motion patterns. The jet-promoted tumble motion depends on factors that determine the intake-induced tumble typical for gasoline-like combustion chamber, e.g. the VVA profile, piston shape and speed. The jet-promoted swirl motion, on the contrary, largely relies on the Coandă effect that in turn depends on the deflection of the gas jet by intake air flow, i.e. the relative position of VVA profile and injection window. Specific to the present combustion chamber with side-mounted tumble-oriented injector, it is therefore concluded that factors influence the mixture formation process through exerting influences on the jet-promoted motion. The only exception is early injection close to the valve-overlapping TDC, wherein the impingement of jet on piston is the major mechanism. And, in fact, the jet-promoted motion resulted from the flat side-mounted injector turns out to have comparable mixing capability to the direct jet-piston impingement. It is in addition found that, as the main mixing mechanism is injection-dependent, the mixing rate is scaled with absolute time rather than crank angle, and the mixture formation process is more critical for high-speed operating points.

Turbulence level is also affected by the injection that, apart from mixture quality, influences the combustion process. It is found that gas injection contributes to combustion-relevant turbulence mainly by intensifying the large-scale charge motion and marginally by generating small-scale vortices around the jet, as far as the side-mounted injector in this work is concerned.

As the design of injector and combustion chamber has been verified and the mixing mechanism and trends identified, a multi-cylinder prototype engine was built to compare the rated torque and power against the reference CNG PFI and target GDI engines. The low-end torque proved critical but the performance gap was bridged thanks to the high mixing capability and advanced VVA profile design. At this point the engine design has been successfully accomplished and the prototype engine is ready for extensive performance and emission analysis on dynamic test bench.

References

1. Cho, H.M. and He, B.Q., "Spark Ignition Natural Gas Engines – a Review," Energy Conv. and Management 48:608-618, 2007, doi:10.1016/j.enconman.2006.05.023.
2. Korakianitis, T., Namasivayam, A.M., and Crookes, R.J., "Natural-Gas Fueled Spark-Ignition (SI) and Compression-Ignition (CI) Engine Performance and Emissions," Progress in Energy and Combustion Science 37(1):89-112, 2011, doi:10.1016/j.pecs.2010.04.002.
3. Economides M.J. and Wood, D.A., "The State of Natural Gas," J. Natural Gas Sci. and Engineering 1(1-2):1-13, 2009, doi:10.1016/j.jngse.2009.03.005.
4. Stepmien, J.P., Ni, M., Sun, Q., and Chan, S.H., "Production of Sustainable Methane from Renewable Energy and Captured Carbon Dioxide with the Use of Solid Oxide Electrolyser: a Thermodynamic Assessment," Energy 82:714-721, 2015, doi:10.1016/j.energy.2015.01.081.
5. Alamia, A., Magnusson, I., Johnsson, F., and Thunman, H., "Well-to-Wheel Analysis of Bio-Methane via Gasification, in Heavy Duty Engines within the Transport Sector of the European Union," Applied Energy 170:445-454, 2016, doi:10.1016/j.apenergy.2016.02.001.
6. Sobiesiak, A. and Zhang, S., "The First and Second Law Analysis of Spark Ignition Engine Fuelled with Compressed Natural Gas," SAE Technical Paper 2003-01-3091, 2003, doi:10.4271/2003-01-3091.
7. Borges, L., Hollnagel, C., and Muraro, W., "Development of a Mercedes-Benz Natural Gas Engine M 366 LAG, with a Lean Burn Combustion System," SAE Technical Paper 962378, 1996, doi:10.4271/962378.
8. Kalam, M.A. and Masjuki, H.H., "An Experimental Investigation of High Performance Natural Gas Engine with Direct Injection," Energy 36(5):3563-3571, 2011, doi:10.1016/j.energy.2011.03.066.
9. Zeng, K., Huang, Z., Liu, B., Liu, L. et al., "Combustion Characteristics of a Direct-Injection Natural Gas engine under Various Fuel Injection Timings," Applied Thermal Engineering 26(8-9):806-813, 2006, doi:10.1016/j.applthermaleng.2005.10.011.
10. Kubesh, J., "Development of a Throttleless Natural Gas Engine," SAE Technical Paper 2001-01-2522, 2001, doi:10.4271/2001-01-2522.
11. Chiodi, M., Berner, H., and Bargende, M., "Investigation on Different Injection Strategies in a Direct-Injected Turbocharged CNG-Engine," SAE Technical Paper 2006-01-3000, 2006, doi:10.4271/2006-01-3000.
12. Douailler, B., Ravet, F., Delpech, V., Soleri, D. et al., "Direct Injection of CNG on High Compression Ratio Spark Ignition Engine: Numerical and Experimental Investigation," SAE Technical Paper 2011-01-0923, 2011, doi:10.4271/2011-01-0923.
13. Mohammed, S., Baharom, M.B., Aziz, A.R., and Firmansyah, "The Effects of Fuel-Injection Timing at Medium Injection Pressure on the Engine Characteristics and Emissions of a CNG-DI Engine Fueled by a Small Amount of Hydrogen in CNG," Int. J. Hydrogen Energy 36(18):11997-12006, 2011, doi:10.1016/j.ijhydene.2011.05.110.
14. Aziz, A. and Firmansyah, "The Effect of Fuel Rail Pressure on the Performance of a CNG-Direct Injection Engine," SAE Technical Paper 2009-01-1498, 2009, doi:10.4271/2009-01-1498.
15. Yadollahi, B. and Boroomand, M., "The Effect of Combustion Chamber Geometry on Injection and Mixture Preparation in a CNG Direct Injection SI Engine," Fuel 107:52-62, 2013, doi: 10.1016/j.fuel.2013.01.004.
16. Keskinen, K., Kaario, O., Nuutinen, M., Vuorinen, V. et al., "Mixture Formation in a Direct Injection Gas Engine: Numerical Study on Nozzle Type, Injection Pressure and Injection Timing Effets," Energy 94:542-556, 2016, doi:10.1016/j.energy.2015.09.121.
17. Schulz, C. and Sick, V., "Tracer-LIF Diagnostics: Quantitative Measurement of Fuel Concentration, Temperature and Fuel/Air Ratio in Practical Combustion Systems," Prog. In Energy and Combustion Sci. 31(1):75-121, 2005, doi:10.1016/j.pecs.2004.08.002.
18. Zhao, H. and Ladommatos, N., "Optical Diagnostics for In-Cylinder Mixture Formation Measurements in IC Engines," Prog. In Energy and Combustion Sci. 24(4):297-336, 1998, doi:10.1016/S0360-1285(98)80026-9.
19. Crist, S., Glass, D.R., and Sherman, P.M., "Study of the Highly Underexpanded sonic jet," AIAA J. 4(1):68-71, 1966, doi:10.2514/3.3386.
20. Donaldson, C.D. and Snedeker, R.S., "A Study of Free Jet Impingement. Part 1: Mean Properties of Free and Impinging Jets," J. Fluid Mechanics 45(2):281-319, 1971, doi:10.1017/S0022112071000053.
21. Baratta, M., Catania, A., Spessa, E., Herrmann, L. et al,. "Multi-Dimensional Modelling of Direct Natural-Gas Injection and Mixture Formation in a Stratified-Charge SI Engine with Centrally Mounted Injector," SAE Int. J. Engines 1(1):607-626, 2009, doi:10.4271/2008-01-0975.
22. Kim, G.H., Kirkpatrick, A., and Mitchell, C., "Computational Modeling of Natural Gas Injection in a Large Bore Engine," J. Eng. Gas Turbines Power 126(3):656-664, 2004, doi:10.1115/1.1762906.
23. Abraham, J., "What is Adequate Resolution in the Numerical Computations of Transient Jets?," SAE Technical Paper 970051, 1997, doi:10.4271/970051.
24. Li, Y., Kirkpatrick, A., Mitchell, C., and Willson, B., "Characteristic and Computational Fluid Dynamics Modeling of High-Pressure Gas Jet Injection," J. Eng. Gas Turbines Power 126(1):192-197, 2004, doi:10.1115/1.1635398.
25. Baratta M. and Rapetto N., "Fluid-Dynamic and Numerical Aspects in the Simulation of Direct CNG Injection in Spark-Ignition Engines," Computers and Fluids 103:215-233, 2014, doi:10.1016/j.compfluid.2014.07.028.
26. Hanjalic, K. and Popovac, M., "A Robust Near-Wall Ellipitic-Relaxation Eddy-Viscosity Turbulence Model for CFD," Int. J. Heat Fluid Flow 25(6):1047-1051, 2004, doi:10.1016/j.ijheatfluidflow.2004.07.005.
27. Popovac, M. and Hanjalic, K., "Compound Wall Treatment for RANS Computation of Complex Turbulent Flows and Heat Transfer," Flow Turbulence Combust. 78(2):177-202, 2007, doi:10.1007/s10494-006-9067-x.
28. Abraham, J., Magi, V., MacInnes, J., and Bracco, F., "Gas versus Spray Injection: Which Mixes Facter?," SAE Technical Paper 940895, 1994, doi:10.4271/940895.

29. Baratta, M., d'Ambrosio, S., Misul, D., and Spessa, E., “Effects of H2 addition to CNG blends on cycle-to-cycle and cylinder-to-cylinder combustion variation in a spark ignition engine” ASME Transactions, Journal of Engineering for Gas Turbines and Power, Vol. 136, pp. 051502-1/12, 2014.
30. Baratta, M., d'Ambrosio, S., and Misul, D., “Performance and Emissions of a Turbocharged Spark Ignition Engine Fueled with CNG and CNG/Hydrogen Blends” SAE Paper No. 2013-01-0866, SAE 2013 World Congress & Exhibition, Detroit (USA), April 16-18, 2013.

Contact Information

MIRKO BARATTA

Dipartimento Energia, Politecnico di Torino

Corso Duca degli Abruzzi 24

10129 Torino – Italy

mirko.baratta@polito.it

+39 011 090 4484

ALOIS FUERHAPTER

AVL LIST GMBH

A-8020 Graz, Hans-List-Platz 1 – Austria

alois.fuerhapter@avl.com

+43 316 787 1499

CESARE PELETTO

Centro Ricerche Fiat S.c.P.A.

Strada Torino 50, 10043 Orbassano (TO), Italy

cesare.peletto@crf.it

+39 011 9083437

PATRICK SALEMI

Delphi Luxembourg SA

Avenue de Luxembourg

L4940 Bacharage

GD Of Luxembourg

patrick.salemi@delphi.com

+352 5018 2470

Definitions/Abbreviations

BDC	bottom dead center
CO	carbon monoxide
CO2	carbon dioxide
CR	compression ratio
degCA	crank angle degree
EOI	end of injection
EVC	exhaust valve closing
EVO	exhaust valve opening
HC	hydrocarbon
IMEP	indicated mean effect pressure
IVC	intake valve closing
IVO	intake valve opening
MFB	mass fraction burned
SA	Spark advance
SOI	start of injection
TDC	top dead center